Quantum approach to nucleation times of kinetic Ising ferromagnets

M. D. Grynberg[1] and R. B. Stinchcombe[2]
[1]*Departamento de Física, Universidad Nacional de La Plata, (1900) La Plata, Argentina*
[2]*Rudolf Peierls Centre for Theoretical Physics, University of Oxford, 1 Keble Road, Oxford OX1 3NP, United Kingdom*
(Received 14 January 2005; published 6 June 2005)

Low temperature dynamics of Ising ferromagnets under finite magnetic fields are studied in terms of quantum spin representations of stochastic evolution operators. These are constructed for the Glauber dynamic as well as for its modification, introduced by Park *et al.* [Phys. Rev. Lett. **92**, 015701 (2004)]. In both cases the relaxation time after a field quench is evaluated both numerically and analytically using the spectrum gap of the corresponding operators. The numerical work employs standard recursive techniques following a symmetrization of the evolution operator accomplished by a nonunitary spin rotation. The analytical approach uses low temperature limits to identify dominant terms in the eigenvalue problem. It is argued that the relaxation times already provide a measure of actual nucleation lifetimes under finite fields. The approach is applied to square, triangular and honeycomb lattices.

DOI: 10.1103/PhysRevE.71.066104 PACS number(s): 64.60.Qb, 02.50.−r, 64.60.My, 75.60.Jk

I. INTRODUCTION

Nucleation phenomena are of basic importance in a wide range of metastable systems which typically involve the crossing of a free energy barrier that is large compared to thermal fluctuations [1]. Classical examples of such situation are the formation of droplets in an undercooled gas or of crystals in an undercooled liquid, whereas numerous analogies can also be found in contexts as diverse as, for instance, material science [2], astrophysics [3], and quantum liquids [4]. Owing to the initial state of these systems, generally produced by a rapid quench from a stable phase, the resulting decay time before escaping from metastability may be extremely large at low temperatures. A significant part of the theoretical understanding of these relaxation processes has been amply developed in the study of kinetic Ising ferromagnets as microscopic (lattice) models of nucleation. In this framework, the metastable phase can be prepared after equilibrating the system under an external magnetic field h which is then suddenly reversed. The system therefore evolves toward the full minimization of its free energy via the formation of droplets or small clusters of spins aligned with the new field direction. These droplets start growing with very small rates until at least one of them exceeds a critical size, i.e., a saddle point configuration or a local maximum in the free energy landscape, thus triggering a rapid magnetization change in the whole system. This stems in part from the competition between the energy gained by aligning spins with the field and the interface energy created in reorienting previously parallel spins; thus escape from metastability essentially occurs when the cost of the latter is outweighted by the gain of the former.

Several analytical studies have been addressed to elucidate the dynamical aspects of these processes in the low temperature limit [5–9] while more recently, the actual evaluation of average nucleation lifetimes has been studied combining a range of numerical and analytical efforts [10–16]. As a further step in this direction, in this work we discuss an alternative low temperature procedure (both numerical and analytical), to estimate the relaxation time τ of Ising ferromagnets evolving through detailed balance stochastic rules [17]. Specifically, we consider both the usual Glauber dynamic [18] along with a seemingly minor modification of the latter which, however, yields entirely different characteristics at large magnetic fields [11]. In either case, we construct a quantum spin representation of the evolution operator whose spectrum gap (τ^{-1}) provides a measure of nucleation rates. In line with the general grounds referred to above, the implicit assumption allowing for this identification is that the first passage time [17] to create randomly a critical nucleus is much longer than the characteristic time scale involved in subsequent growth [19]. Thus, the relaxation of the entire system can be expected to coincide with the inverse of the probability of escaping from the metastable well. *A posteriori*, our results will lend further support to this view.

Another assumption that is usually made in homogeneous systems—and which is crucial for the feasibility of our numerical approach—is that multi spin-flip events as well as fusion between subcritical clusters are vanishingly rare in the low temperature limit [1,5]. This is supported by our analytic work. Therefore, the relevant length scale over which the slow part of the dynamic takes place is of the order of a critical droplet size, the first one to nucleate. Although on one hand this prevents us from dealing with small field regimes, where the nucleus becomes macroscopic in the limit $h \to 0$; on the other hand this enables us to study other h regions using numerically accessible clusters, so long as the nucleus can be contained in them. This does not presuppose a precise knowledge of either the nucleus size and shape (sometimes a conceptual problem of its own [7,20]), or the most probable path during a nucleation event [5,7], so in this regard our numerical and analytical procedures provide a complementary approach to that of absorbing Markov chains [17] and other related techniques discussed in Refs. [10,11,14,16].

For two-dimensional lattices and low temperatures T, the average nucleation time $\tau(h,T)$ we aim to evaluate has been rigorously shown to be parametrizable as [5]

$$\tau = A(h)\exp[\beta\Gamma(h)]; \tag{1}$$

thus, the temperature dependence enters solely in the factor $1/\beta = k_B T$ (hereafter the Boltzmann constant k_B is set equal to 1). Independently of the stochastic dynamic considered, the exponential argument Γ has been often associated with the energy barrier separating the saddle point from the metastable phase. In fact, for the Glauber dynamics the analysis of Ref. [5] corroborates this issue. However, the results of Refs. [10,11] clearly indicate that this interpretation of Γ is not always correct, even though the geometry of the critical droplets remains unaltered by the change of dynamic. In particular, for the modified Glauber (MG) dynamics considered there [21], and to be discussed in the following sections, despite detailed balance the value of Γ does not actually yield that energy barrier. Moreover, under strong magnetic fields the nucleation process led by the MG dynamics turns out to remain active (i.e., $\Gamma > 0$), whereas above a maximum field the standard Glauber dynamic just exhibits a fast decay ($\Gamma \equiv 0$). As for the amplitudes A of Eq. (1), as well as for those involved in the nucleation times of a variety of systems [1,13], they have been usually difficult to evaluate numerically given their subdominant contribution. However, the lack of a fair estimation of these prefactors may introduce far reaching theoretical implications in the nucleation picture [22]. Recent efforts have been addressed to remedy this situation in the context of Ising ferromagnets under finite fields [10,11,13,16]. On departing from the low temperature regime assumed in Eq. (1), these amplitudes have revealed a structure of narrow peaks [13] which, however, rapidly collapses toward a piecewise constant function of h in the limit $T \to 0$. Their actual values also turn out to be dynamics dependent [10,11]. Here, we numerically estimate the Γ and A parameters under finite fields using both the Glauber and MG dynamics introduced in Ref. [11]. To check the reliability of our numerical operational approach we compare its results with those obtained in square lattices [5,11], and then proceed further in honeycomb and triangular lattices where no results are previously available to our knowledge. One can expect that in addition to the evolution details, the relaxation parameters will be also affected by the lattice structure as it determines the geometry of the critical droplets ultimately controlling the nucleation time [5,7]. Apart from the square lattice, their size and shape are not known *a priori* but neither is needed in our procedure. Our low temperature analytic work provides results for Γ and A parameters generally in good agreement with their numerical estimates.

The layout of this work is organized as follows. In Sec. II we recast the master equation governing the probability distribution of these processes in terms of a quantum spin analogy whose "Hamiltonian" provides the appropriate transition rates between the original Ising spin configurations. By means of an ulterior nonunitary spin rotation, this results in a symmetric representation of the evolution operator. This simplifies considerably the subsequent numerical analysis of Sec. III in which the spectrum gap of this latter representation is obtained via standard recursive techniques [23] in several situations. In Sec. IV we develop the analytical approach, in which low temperature limits are used to pick out dominant terms in the hierarchy of equations obtained by applying the quantum spin Hamiltonian to an appropriate metastable state. We end the paper with Sec. V which contains our conclusions along with some remarks on extensions of this work.

II. DYNAMICS AND OPERATORS

Let us then consider an Ising ferromagnet with uniform nearest neighbor (NN) interactions $J > 0$ between the spins $s = \pm 1$ of a regular d-dimensional lattice. Under an applied magnetic field h, taken positive from now on, the corresponding Hamiltonian reads

$$\mathcal{H}_I = -J \sum_{\langle \mathbf{r},\mathbf{r}' \rangle} s_{\mathbf{r}} s_{\mathbf{r}'} - h \sum_{\mathbf{r}} s_{\mathbf{r}}, \tag{2}$$

where the first and second sums run, respectively, over all NN or bond pairs $\langle \mathbf{r},\mathbf{r}' \rangle$, and all spin locations $\mathbf{r}$ of the lattice. Since $\mathcal{H}_I$ actually defines a classical energy functional, the constituent spins do not have a natural dynamics, i.e., $\partial_t s_{\mathbf{r}} = [\mathcal{H}_I, s_{\mathbf{r}}] \equiv 0$. Consequently, a specific stochastic evolution must be prescribed so as to emulate the interactions between the spins and a heat bath, here modeling the fast degrees of freedom not included in the classical Hamiltonian $\mathcal{H}_I$. As usual, the underlying nonequilibrium dynamics is then approximated by a discrete Markovian process and therefore described by a master equation. The latter governs entirely the time evolution of the probabilities $P(s,t)$ of finding the system in a certain spin configuration $|s\rangle$ at time t. If $W(s \to s')$ denotes the (time independent) rate or transition probability per unit time at which configuration $|s\rangle$ evolves to $|s'\rangle$, the master equation just adopts the continuity form

$$\partial_t P(s,t) = \sum_{s'} [W(s' \to s)P(s',t) - W(s \to s')P(s,t)]. \tag{3}$$

Because in the context of Sec. I metastability is imposed by an external field, among the decay processes representable by Eq. (3) we restrict our attention to those in which the total magnetization is not preserved [24]. One of the most studied examples of this type is the Glauber dynamic [18]. Its transition rates involve Ising configurations differing at most in the state of a spin at a given site $\mathbf{r}$. With the aid of the local field variables, which henceforth we define as $\varphi_{\mathbf{r}} = (J/T)\Sigma_{\langle \mathbf{r},\mathbf{r}' \rangle} s_{\mathbf{r}'}$, these rates can be written as

$$W_G(s_{\mathbf{r}} \to -s_{\mathbf{r}}) = [1 + e^{2(\varphi_{\mathbf{r}} + H)s_{\mathbf{r}}}]^{-1}, \tag{4}$$

where $H = h/T$. The iteration of these rules eventually bring the system to the Gibbs distribution as they clearly satisfy detailed balance in Eq. (3), that is, $W(s \to s')e^{-\mathcal{H}_I\{s\}} = W(s' \to s)e^{-\mathcal{H}_I\{s'\}}$. However, other single-spin-flip or Glauber type processes can also be made consistent with these latter conditions, so the approach to equilibrium in these problems is not unique. As was referred to above, a recent case of this situation was introduced in Ref. [11] with the aim of clarifying earlier issues of metastable lifetimes. In the MG dynamics proposed there, the effects of the J interactions and the field h are factorized in the transition rates. More specifically, these are given by [25]

$$W_{MG}(s_{\mathbf{r}} \to -s_{\mathbf{r}}) = [1 + e^{2\varphi_{\mathbf{r}} s_{\mathbf{r}}}]^{-1}[1 + e^{2Hs_{\mathbf{r}}}]^{-1}. \quad (5)$$

Although it can be easily checked that such rates also comply with detailed balance, it will turn out that each of the above dynamics behaves quite differently under strong field regimes.

A. Mean field excursus

Before constructing a more convenient representation for these processes, we pause briefly to consider this latter dynamic at a simple mean field level of description. Despite being quantitatively uncontrolled, on the other hand it is able to account for some relevant qualitative features actually occurring in the MG dynamics (see Secs. III and IV). Thus, in order to decouple the rather involved hierarchy of equations implicit in Eq. (3) we simply approximate the local field variables $\varphi_{\mathbf{r}}$ by their mean value $z\langle s\rangle J/T$, in turn assumed to be homogeneous. Here, $\langle s\rangle$ denotes the average magnetization whereas z stands for the number of NN spins, i.e., the lattice coordination number. After inserting the so approximated W_{MG} rates in Eq. (3), we readily obtain the magnetization dynamics in terms of a nonlinear differential equation which at finite fields and low temperature regimes reduces to

$$\partial_t\langle s\rangle = \frac{1 - \langle s\rangle}{1 + e^{-2z\langle s\rangle J/T}}, \quad h/T \gg 1. \quad (6)$$

Hence, for the region of our interest the relaxation dynamics comes out to be field independent in this scheme. Although this is not the actual case below a minimum h value (see results of Secs. III and IV), yet the analysis of Eq. (6) pinpoints a genuine difference with respect to the Glauber dynamics. Notice that for this latter, if $h/J > z$, in the limit $T \to 0$ the resulting master equation is totally decoupled by the Glauber rates (4), just as if the spins were independent. Then, it follows that $\partial_t\langle s\rangle = 1 - \langle s\rangle$, and therefore the time scale of the Glauber problem is of the order of an elementary step, namely, $\tau = 1$ (see also Sec. III). By contrast, in Eq. (6) the magnetization evolves initially with a much slower pace as its change is exponentially plunged by the initial metastable phase. In fact, the integration of the reciprocal of Eq. (6) between $\langle s\rangle = -1$ and a subsequent magnetization $\langle s\rangle > -1$ involves large escape times. More precisely, with the aid of the exponential-integral function $\mathrm{Ei}(\langle s\rangle)$ and its asymptotic expansions [26], we obtain

$$\tau \sim \frac{T}{4zJ} e^{2zJ/T}, \quad T/J \ll 1. \quad (7)$$

This is consistent with a value of $\Gamma = 2zJ$ in Eq. (1) which later on will be corroborated both numerically (Sec. III) as well as analytically (Sec. IV). The corresponding amplitudes, however, are significantly underestimated by this mean field simplification which nevertheless is already able to capture the metastability of MG dynamics, at least under strong field conditions.

B. Quantum spin representations

We now build up an alternative representation of Eq. (3) lending itself more readily for a numerical study in finite spin clusters which, as pointed out in Sec. I can embody the nucleation time of much larger systems. First, it is useful to recall the matrix elements of the evolution operator $\mathcal{H}$ associated with a generic Markovian process. In terms of transition rates, these elements are constructed as [17]

$$\langle s'|\mathcal{H}|s\rangle = -W(s \to s'), \quad s \neq s', \quad (8)$$

$$\langle s|\mathcal{H}|s\rangle = \sum_{s' \neq s} W(s \to s'). \quad (9)$$

This permits us to think of the master equation in imaginary time as a Schrödinger-like representation $|P(t)\rangle = e^{-\mathcal{H}t}|P(0)\rangle$ in which the probability distribution $|P(t)\rangle = \Sigma_s P(s,t)|s\rangle$ evolves according to the action of the evolution operator—here playing the role of the Hamiltonian—on the initial state $|P(0)\rangle$ (in our case, a metastable Gibbs distribution opposing the new field direction). The specific form of $\mathcal{H}$ in either of the above dynamics can be straightforwardly found in terms of spin-$\frac{1}{2}$ Pauli matrices $\vec{\sigma}$ and interpreting the local field variables involved in Eqs. (4) and (5) as local field operators $\varphi^z_{\mathbf{r}}$:

$$\varphi^z_{\mathbf{r}} = \frac{J}{T} \sum_{\langle \mathbf{r},\mathbf{r}'\rangle} \sigma^z_{\mathbf{r}'}, \quad (10)$$

which just for convenience are taken diagonal, say in the σ^z representation. To connect two z configurations of spins differing in the state of site $\mathbf{r}$, and therefore to account for the off diagonal elements (8), we simply project the corresponding "rate operator" (set by $\varphi^z_{\mathbf{r}}$), in terms of the usual spin raising and lowering projectors $\sigma^+_{\mathbf{r}}, \sigma^-_{\mathbf{r}}$. For example, using the Glauber rates (4), the operational counterpart of Eq. (8) will read

$$\sum_{s,s',s\neq s'} |s'\rangle\langle s'|\mathcal{H}_G|s\rangle\langle s| = -\sum_{\mathbf{r}} \{\sigma^+_{\mathbf{r}}[1 + e^{-2(\varphi^z_{\mathbf{r}} + H)}]^{-1} + \sigma^-_{\mathbf{r}}[1 + e^{2(\varphi^z_{\mathbf{r}} + H)}]^{-1}\}. \quad (11)$$

Since $[\varphi^z_{\mathbf{r}}, \sigma^\pm_{\mathbf{r}}] = 0$, the above ordering of application is immaterial. On the other hand, conservation of probability requires the emergence of the diagonal elements (9). They basically count the number of ways in which a given configuration $|s\rangle$ can evolve to different states $|s'\rangle$ through a single spin flip. This can be properly tracked down by using the number operators $\hat{n}_{\mathbf{r}} = \sigma^+_{\mathbf{r}}\sigma^-_{\mathbf{r}}$ along with the weighting of each flip with its corresponding rate. For the Glauber case the analog of Eq. (9) then becomes

$$\sum_s |s\rangle\langle s|\mathcal{H}_G|s\rangle\langle s| = \sum_{\mathbf{r}} \{\hat{n}_{\mathbf{r}}[1 + e^{2(\varphi^z_{\mathbf{r}} + H)}]^{-1} + [1 - \hat{n}_{\mathbf{r}}][1 + e^{-2(\varphi^z_{\mathbf{r}} + H)}]^{-1}\} = \frac{1}{2}\sum_{\mathbf{r}} [1 - \sigma^z_{\mathbf{r}} \tanh(\varphi^z_{\mathbf{r}} + H)], \quad (12)$$

which together with Eq. (11) completes the form of $\mathcal{H}_G$. Certainly, the above reasoning is extensible to the MG dy-

namic as well. The related evolution operator $\mathcal{H}_{MG}$ of this case thus finally turns out to be

$$\mathcal{H}_{MG} = -\frac{1}{2}\,\mathrm{sech}\,H\sum_{\mathbf{r}}\left[\sigma_{\mathbf{r}}^{+}e^{H}(1+e^{-2\varphi_{\mathbf{r}}^{z}})^{-1}+\sigma_{\mathbf{r}}^{-}e^{-H}(1+e^{2\varphi_{\mathbf{r}}^{z}})^{-1}\right] + \frac{1}{4}\sum_{\mathbf{r}}(1-\sigma_{\mathbf{r}}^{z}\tanh\varphi_{\mathbf{r}}^{z})(1-\sigma_{\mathbf{r}}^{z}\tanh H), \tag{13}$$

which of course reduces to $\mathcal{H}_G$ when $h=0$ [25]. Also, it can be easily verified that either of these operators remains invariant under the spin inversion $\sigma^z \to -\sigma^z$ along with the field reversal $h \to -h$, as they should. Given the rather involved manner in which all spins are coupled through the local field operators $\varphi_{\mathbf{r}}^{z}$, exact analytic treatments of the spectrum of $\mathcal{H}_G$ or of $\mathcal{H}_{MG}$ under generic field and temperature conditions may seem unlikely, even in $d=1$ [27]. However, by exploiting low temperature limits analytic procedures can be developed and applied, as shown in Sec. IV. In addition, numerical progress can be made in fair system sizes by means of a suitable similarity transformation which we now discuss.

C. Symmetric representations

As is known [17], the detailed balance property of rates (4) and (5) warrants the existence of representations in which $\mathcal{H}_G$ and $\mathcal{H}_{MG}$ are symmetric and thereby diagonalizable. Moreover, a *common* transformation for that purpose can be found for both dynamics. To this end, we rotate the corresponding operators around the z spin direction using a site dependent pure imaginary angle

$$\phi_{\mathbf{r}} = -i(\varphi_{\mathbf{r}} + H), \tag{14}$$

where the φ's are the original scalar fields introduced in Eqs. (4) and (5). This rotation is produced by the nonunitary similarity transformation $U=e^{-iS}$ with $S=\frac{1}{2}\Sigma_{\mathbf{r}}\phi_{\mathbf{r}}\sigma_{\mathbf{r}}^{z}$, which in turn results in the direct product

$$U = \bigotimes_{\mathbf{r}} U_{\mathbf{r}}, \quad U_{\mathbf{r}} = \begin{bmatrix} e^{-(\varphi_{\mathbf{r}}+H)/2} & 0 \\ 0 & e^{(\varphi_{\mathbf{r}}+H)/2} \end{bmatrix}. \tag{15}$$

While the diagonal terms of $\mathcal{H}_G$ and $\mathcal{H}_{MG}$ remain unaltered by U, it is straightforward to show that

$$U\sigma_{\mathbf{r}}^{\pm}U^{-1} = e^{\mp(\varphi_{\mathbf{r}}+H)}\sigma_{\mathbf{r}}^{\pm}. \tag{16}$$

From this latter relation, one can immediately verify that the rotated Glauber operator $\mathcal{H}'_G = U\mathcal{H}_G U^{-1}$ can finally be cast in the symmetric form

$$\mathcal{H}'_G = \frac{1}{2}\sum_{\mathbf{r}}\left[1-\sigma_{\mathbf{r}}^{z}\tanh(\varphi_{\mathbf{r}}^{z}+H)-\sigma_{\mathbf{r}}^{x}\,\mathrm{sech}(\varphi_{r}^{z}+H)\right], \tag{17}$$

whereas the rotated version $\mathcal{H}'_{MG} = U\mathcal{H}'_{MG}U^{-1}$ of the MG dynamics is also symmetric and comes out to be

$$\mathcal{H}'_{MG} = \frac{1}{4}\sum_{\mathbf{r}}\left[(1-\sigma_{\mathbf{r}}^{z}\tanh\varphi_{\mathbf{r}}^{z})(1-\sigma_{\mathbf{r}}^{z}\tanh H) - \sigma_{\mathbf{r}}^{x}\,\mathrm{sech}\,\varphi_{\mathbf{r}}^{z}\,\mathrm{sech}\,H\right]. \tag{18}$$

The formal analogy with the Schrödinger picture referred to above now becomes more transparent, as all solutions of the master equation are necessarily obtained as superpositions of eigenstates $|\psi_\lambda\rangle$ with *real* eigenvalues (or energies) $\lambda \geqslant 0$ of Hermitian Hamiltonians. In particular, the ground states $|\psi_0\rangle$ of both $\mathcal{H}'_G$ and $\mathcal{H}'_{MG}$ coincide and are closely related to the equilibrium Gibbs distribution. This is because $\langle\tilde{\psi}| \equiv \Sigma_s\langle s|$ is the *left* steady state of the original stochastic operators (notice that their columns add up to zero), and therefore $\langle\psi_0| = \langle\tilde{\psi}|U^{-1} = \Sigma_s\langle s|e^{-\beta\mathcal{H}_I\{s\}/2}$, modulo a normalization factor $\sqrt{Z}$ involving the partition function of the Ising energies (2). It is thereby a simple matter to check that in our symmetric representation the dynamics of any classical quantity $\mathcal{A}$ (which is already diagonal in the σ^z representation, such as the magnetization, the energy $\mathcal{H}_I$, or any microscopic correlator) can be written as

$$\langle\mathcal{A}\rangle(t) = \frac{1}{Z}\sum_{s}\mathcal{A}\{s\}e^{-\beta\mathcal{H}_I\{s\}} + \sum_{\lambda>0}e^{-\lambda t}\langle\tilde{\psi}|U^{-1}\mathcal{A}|\psi_\lambda\rangle \times\langle\psi_\lambda|U|P(0)\rangle. \tag{19}$$

Thus, we see that the relaxation times discussed throughout Sec. I can be read off from the first excited level of the evolution operators constructed so far and whose numerical analysis we next turn to consider.

III. NUMERICAL RESULTS

The main advantage of the symmetric representations (17) and (18) is that their lower eigenmodes, which are just the ones dominating the above nonequilibrium terms, can be efficiently computed using recursion-type algorithms devised for Hermitian matrices, e.g., the Lanczos technique [23]. The latter is particularly appropriate to study system sizes capable of accommodating critical droplets arising from not too small field regimes. Specifically, for a *square* lattice the critical nucleus is an $\mathcal{L}\times(\mathcal{L}-1)$ rectangle of overturned spins gathered to a similar spin on one of its long sides of length $\mathcal{L}=[2J/h]$, where $[\,]$ denotes the integer part [5]. Hence, in line with the general arguments of Sec. I one could expect that for $h/J \gtrsim 0.5$ a spectrum gap of at least a 5×4 spin system will suffice to yield actual values of nucleation times in the low temperature limit.

Thus, starting from a random initial state but chosen orthogonal to the Gibbs-like distribution $|\psi_0\rangle$ referred to above, we carried out the standard Lanczos procedure in such spin clusters using periodic boundary conditions (hereafter, assumed throughout this section). Let us first consider the Glauber operator (17). In Fig. 1 we show the results obtained from its first excitation level λ_1, i.e., above equilibrium, when varying the field $h/J \in (1,4)$ at low temperature regimes $T/J \sim 0.2$–0.4. The nucleation time parametrization conjectured by Eq. (1), here identified with $1/\lambda_1$, is consistent with both the data collapse in the main panel as well as with the linear behavior evidenced in the inset. In particular, the slopes of the latter detect three typical amplitude values which in turn are used as scaling factors in the main panel, thus producing, as expected, the collapse of different curves.

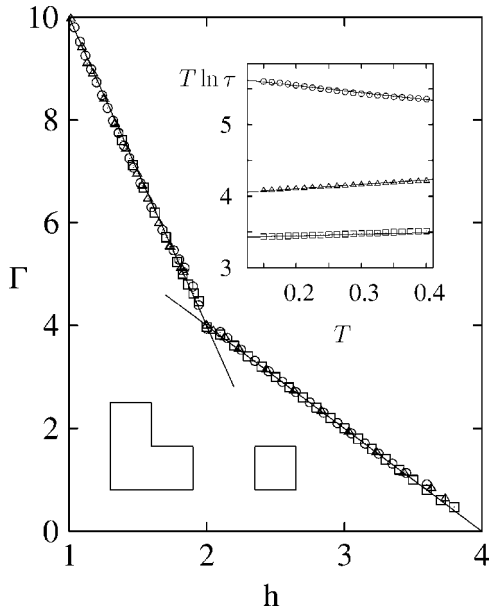

FIG. 1. Low temperature estimation of the relaxation parameters $\Gamma \equiv T \ln(\tau/A)$ in square lattices for $T=0.2$ (squares), 0.3 (triangles), and 0.4 (circles) resulting from the Lanczos diagonalization of Eq. (17) in small clusters (up to 6×4 spins). Solid lines denote the estimations of Eq. (20). The data collapse was attained upon using the amplitudes $A=e^s$ derived from the slopes s of the upper inset. From top to bottom they refer respectively to $h=1.7$, 2, and 2.3, characterizing typical regimes of Eq. (17). The lower lines sketch the shape of the critical droplets for $1<h<2$ (three spins) and $2<h<4$ (single spin). Here and in all subsequent figures, T, h, and Γ are measured in units of the exchange couplings J.

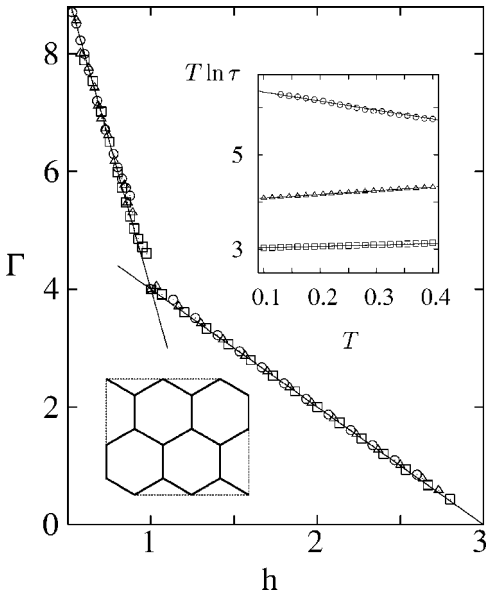

FIG. 2. Relaxation parameters of honeycomb lattices estimated from the diagonalization of Eq. (17) using the 18-spin cluster depicted by the lower inset. As in Fig. 1, the amplitudes yielding the data collapse in the main panel [$T=0.2$ (squares), 0.3 (triangles), and 0.4 (circles)] were inferred from the slopes of the upper inset. The latter refer respectively to $h=0.75$ (top), 1 (middle), 1.5 (bottom) and are representative of the field regimes summarized in Eq. (21) (solid lines of main panel).

After a least square linear fitting of our data, the corresponding relaxation parameters within the above temperature and field ranges are found to be

$$\Gamma_G \sim \begin{cases} 16.(1)J - 6.(0)h, & 1 \lesssim \dfrac{h}{J} < 2, \\ 8.(1)J - 2.(0)h, & 2 \leqslant \dfrac{h}{J} \lesssim 4, \end{cases}$$

$$A_G \sim \begin{cases} 0.4(3), & 1 \lesssim \dfrac{h}{J} < 2, \\ 1.9(4), & \dfrac{h}{J} = 2, \\ 1.3(3), & 2 < \dfrac{h}{J} \lesssim 4. \end{cases} \tag{20}$$

It should be mentioned that *below* $T/J \sim 0.1$ and $h/J \sim 1$, the spectrum gap gradually becomes comparable to the numerical propagation of our roundoff errors, while the convergence of the Lanczos recursion becomes slow and erratic. Nonetheless, above those regimes, where these problems do not show up, our results are already in fair agreement with those of Ref. [11] as well as with the low temperature analysis of Sec. IV. As conjectured earlier, size effects are negligible around this field region, at least judging from 3×3, 4×4, and preliminary results in 6×4 spin arrays, all of which can enclose the critical droplets depicted in Fig. 1. In this regard, notice that the corresponding values of Γ_G are consistent with both the surface tension and magnetic energy of such droplets, in turn recovering the interpretation of Γ as an energy barrier. Also by approaching the decoupling condition $h/J=z$ from below, the low lying levels, which were nondegenerate so far, closely approach one another, as they should, whereas $\Gamma_G \to 0$.

Bolstered by these consistency checks, we now turn our procedure to honeycomb and triangular lattices for which these nucleation parameters are not previously available (see also Sec. IV). Due to the roundoff limitations mentioned above, we restricted the computations respectively to $h/J \gtrsim 0.5$, $T/J \gtrsim 0.1$ and $h/J \gtrsim 1.5$, $T/J \gtrsim 0.3$. For the first situation, Fig. 2 displays the results so obtained in an 18-spin honeycomb cluster (schematized by its lower inset). These are in line with the parametrization (1), and for which our numerical estimations yield

$$\Gamma_G \sim \begin{cases} 14.(1)J - 10.(1)h, & 0.5 \lesssim \dfrac{h}{J} < 1, \\ 6.(0)J - 2.(0)h, & 1 \leqslant \dfrac{h}{J} \lesssim 3, \end{cases} \tag{21}$$

$$A_G \sim \begin{cases} 0.1(6), & 0.5 \lesssim \dfrac{h}{J} < 1, \\ 2.2(1), & \dfrac{h}{J} = 1, \\ 1.3(3), & 1 < \dfrac{h}{J} \lesssim 3. \end{cases}$$

Preliminary tests using 24-spin clusters showed no substantial differences with these results. This conforms with the fact that within our accessible lower field bounds, the above Γ_G's at most can entail a five-spin nucleus (assuming the usual Γ interpretation still holds). However, the shape of this nucleus cannot be inferred only from its surface tension $(14J)$ as z is not large enough. In contrast, the results of the triangular lattice lend themselves more readily for this purpose, at least for the field range shown in Fig. 3. After analyzing 4×4 and 5×4 triangular clusters, in this case further cusps in Γ and amplitude discontinuities are detected, namely,

$$\Gamma_G \sim \begin{cases} 32.(1)J - 10.(1)h, & 1.5 \lesssim \dfrac{h}{J} < 2, \\ 20.(0)J - 4.(0)h, & 2 \lesssim \dfrac{h}{J} < 4, \\ 12.(0)J - 2.(0)h, & 4 \lesssim \dfrac{h}{J} \lesssim 6, \end{cases}$$

$$A_G \sim \begin{cases} 0.7(0), & 1.5 \lesssim \dfrac{h}{J} < 2, \\ 1.(0), & \dfrac{h}{J} = 2, \\ 0.4(5), & 2 < \dfrac{h}{J} < 4, \\ 1.4(2), & \dfrac{h}{J} = 4, \\ 1.2(2), & 4 < \dfrac{h}{J} \lesssim 6. \end{cases} \tag{22}$$

Next, we consider the modified Glauber operator (18). In all studied situations, its numerical treatment comes out to be numerically more demanding, i.e., spectrum gaps are even smaller than before, particularly below $h/J=z-2$. So we limit our computations to $h/J \gtrsim 1$, $T/J \gtrsim 0.2$ for square, $h/J \gtrsim 0.3$, $T/J \gtrsim 0.2$ for honeycomb, and $h/J \gtrsim 2$, $T/J \gtrsim 0.3$ for triangular lattices. Despite these restrictions, the results of Fig. 4 clearly support larger values of $\Gamma(h)$ than those obtained for the Glauber dynamic. Also, the amplitude values turn out to be different as well as their regimes of validity. Specifically, for the square lattice [Fig. 4(a)], we find

$$\Gamma_{MG} \sim \begin{cases} 16.(1)J - 4.(0)h, & 1 < \dfrac{h}{J} < 2, \\ 8.(0)J, & \dfrac{h}{J} \geqslant 2, \end{cases}$$

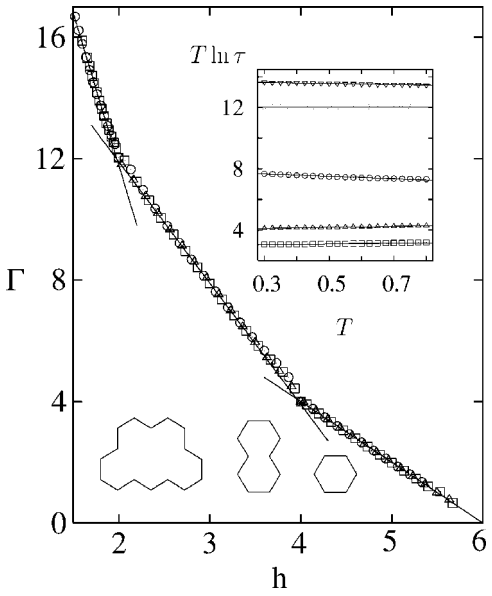

FIG. 3. Relaxation parameters of triangular lattices arising from the gap of Eq. (17) in 4×4 and 5×4 spin clusters. As before, the data collapse was obtained from the slopes of the upper inset. The former refers to $[T=0.3$ (triangles), 0.4 (squares), and 0.5 (circles)], and follows closely the field regimes given in Eq. (22), denoted by solid lines. The amplitudes resulting from the inset slopes are characteristic of the regimes identified in Eq. (22). Here, they refer to $h=1.8$, 2, 3, 4, and 4.5, in descending order. The size and shape of critical droplets are schematized below. From left to right they refer to five spins $(1.5\lesssim h<2)$, two spins $(2<h<4)$, and a single spin $(4<h<6)$.

$$A_{MG} \sim \begin{cases} 0.2(3), & 1 < \dfrac{h}{J} < 2, \\ 1.4(2), & \dfrac{h}{J} = 2, \\ 1.(0), & \dfrac{h}{J} > 2, \end{cases}$$

whereas for honeycomb [Fig. 4(b)] and triangular [Fig. 4(c)] systems the respective parameters become

$$\Gamma_{MG} \sim \begin{cases} 14.(1)J - 8.(0)h, & 0.3 \lesssim \dfrac{h}{J} < 1, \\ 6.(0)J, & \dfrac{h}{J} \geqslant 1, \end{cases}$$

$$A_{MG} \sim \begin{cases} 0.1(3), & 0.3 \lesssim \dfrac{h}{J} < 1, \\ 1.6(6), & \dfrac{h}{J} = 1, \\ 1.(0), & \dfrac{h}{J} > 1, \end{cases} \tag{24}$$

and

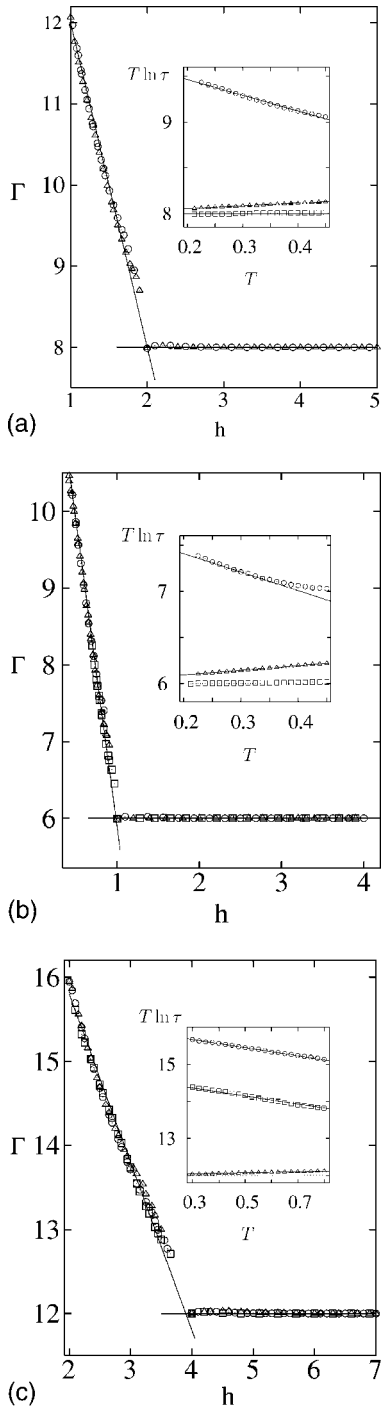

FIG. 4. Relaxation parameters of (a) square, (b) honeycomb, and (c) triangular lattices under the *modified* Glauber dynamics given in Eq. (5). Solid lines in each case stand, respectively, for the regimes identified in Eqs. (23)–(25). In (a) and (b) they follow closely the data of $T=0.4$ (circles), 0.3 (triangles), and, 0.2 (squares), obtained from the numerical diagonalization of Eq. (18); and similarly for (c), where the points denote $T=0.8$ (triangles), 0.6 (circles), and, 0.4 (squares). In contrast to the standard Glauber dynamics, here the relaxation process remains active at large fields, i.e., $\Gamma>0$ for $h\gg J$. As before, the amplitudes were derived from the slopes of the insets. In descending order they refer respectively to (a) $h=1.5,2,2.5$, (b) $h=0.75,1,1.5$, and (c) $h=2,2.5,4,5$ (horizontal line), typical cases of each situation.

$$\Gamma_{MG}\sim\begin{cases}20.(1)J-2.(0)h, & 2\lesssim\dfrac{h}{J}<4,\\ 12.(0)J, & \dfrac{h}{J}\geqslant 4,\end{cases}$$

$$A_{MG}\sim\begin{cases}0.3(4), & 2\lesssim\dfrac{h}{J}<4,\\ 1.1(6), & \dfrac{h}{J}=4,\\ 1.(0), & \dfrac{h}{J}>4.\end{cases} \tag{25}$$

It is worth remarking that, as before, the square lattice parameters are in reasonable agreement with those of Ref. [11], which lends us further confidence in the identification of $1/\lambda_1$ with the nucleation time of the system. Since in all studied cases $\Gamma_{MG}(h)>\Gamma_G(h)$, notice that the usual association of Γ with an energy barrier no longer applies for this dynamics [10,11]. Also, these results give evidence that the nucleation process persists at large times and fields, i.e., $\Gamma_{MG}=2Jz>0$, as opposed to the Glauber picture where $\tau=1$ beyond $h/J=z$. Other tests using much larger fields suggest an identical behavior (see also Sec. IV), always maintaining a nondegenerate level λ_1.

Finally, we point out that errors throughout all A's might be actually larger than those estimated above, given their subdominant contribution to τ in Eq. (1), especially within the smaller field regions. This is reflected in the low sensitivity of the data collapse to amplitude changes slightly away from their error bands (arising only from upper insets).

IV. LOW TEMPERATURE ANALYSIS

Here we develop a low temperature analysis, starting from the quantum formulation of Sec. II, which provides analytic results for the relaxation parameters Γ and A. The method employs the unsymmetrized Hamiltonian

$$\mathcal{H}=-\sum_r\left[(\sigma_r^+-\mathrm{P}_r^-)R^+\left(\sum_{r'}\sigma_{r'}^z\right)+(\sigma_r^--\mathrm{P}_r^+)R^-\left(\sum_{r'}\sigma_{r'}^z\right)\right], \tag{26}$$

where r' are the neighbors of r, and $P_r^{\pm}\equiv\frac{1}{2}(1\pm\sigma_r^z)$. Low temperature versions of the appropriate rates $R^{\pm}(m)$ are used. Here, and throughout, m is an integer corresponding to the "total spin" of the neighbors, and $\pm$ relates to flip up or down. The unsymmetrized form of $\mathcal{H}$ is easier to work with because the low temperature forms of the rates there are nicely separated.

With $|n\rangle$ the amplitude corresponding to a domain of n up spins in the eigenfunction for eigenvalue s, the eigenvalue problem involves a hierarchy of equations relating $|n\rangle$ to $|n\pm1\rangle$, each of which is of the following schematic form:

$$[c_nR^+(\cdots)+d_nR^-(\cdots)-s]|n\rangle = c_nR^+(\cdots)|n+1\rangle+d_nR^-(\cdots)|n-1\rangle. \tag{27}$$

Here the coefficients c_n and d_n depend on geometric factors

of the lattice such as its coordination number z. These equations are consistent with an equal amplitude eigenstate with eigenvalue $s=0$. We want the next eigenvalue, i.e., the "gap" $s=(Ae^{\beta\Gamma})^{-1}$.

The relaxation from a metastable state, which we take to have all spins down (i.e., antiparallel to the field), is governed by the slow rates, especially the slow up-flip rates. Which rates are small depends on the field, so different field regimes have to be considered separately. The first equation ($n=0$) has $d_0=0$, i.e., the only terms come from $c_0R^+(\cdots)=R^+(-z)$, corresponding to nucleation of a single up spin, which state has amplitude $|1\rangle$. The only case where $R^+(-z)$ is not small at low temperatures is the Glauber dynamics case with $zJ<h$, where $R^+(m)\sim 1$ for all m. The equations then give the gap of order 1, so

$$\Gamma_G = 0, \quad h/J > z. \tag{28}$$

In all other cases $R^+(-z)$ is exponentially small in β at low temperatures, and this results in nonzero Γ for Glauber dynamics (G) with $zJ>h$ and for modified Glauber dynamics at any h. So we confine our attention hereafter to those cases, at very low temperatures. Then, $R^+(-z)$ is by far the smallest of the flip-up rates [since for any positive integer l, for MG dynamics $R^+(-l)\sim e^{-2\beta lJ}\ll 1$, while in the Glauber case, if $h<lJ$ then $R^+(-l)\sim e^{-2\beta(lJ-h)}\ll 1$]. Consequently we may neglect terms involving further factors of $R^+(-z)$, as occur, corresponding to further nucleations of isolated single-spin clusters, in the equations for $n>0$. As a result, in Eq. (27), for amplitudes $|n\geqslant 2\rangle$, it is only necessary to consider "connected clusters" where all up spins have at least one up-spin neighbor. For example the second equation ($n=1$) has $c_1R^+(\cdots)=zR^+(-(z-2))$ and $d_1R^-(\cdots)=R^-(-z)$ after neglecting the further nucleation terms involving $R^+(-z)$.

While basic ideas and procedures are similar for G and MG dynamics, because of the different forms of their rates, the ordering of terms in the equations can be different in some regimes, so we discuss the two cases separately, beginning with the Glauber case.

A. Glauber dynamics

Case (a). This includes d-dimensional lattices with $zJ>h>(z-2)J$. Here $R^+(-z)\sim e^{-2\beta(zJ-h)}\ll 1$, and all other $R^+(m)\sim 1$ while $R^-(-z)\sim 1$.

The resulting recursion type eigenequations have (as always) the equal amplitude solution with $s=0$, and (because the only small R^+ occurring is in the first equation) the next eigenvalue satisfies (in the low temperature limit) $[R^+(-z)-s](z+1-s)=R^+(-z)$, giving $s=z(z+1)^{-1}e^{-2\beta(zJ-h)}=(Ae^{\beta\Gamma})^{-1}$. So

$$\Gamma_G = 2(zJ-h), \quad A_G=(z+1)/z, \tag{29}$$

for $zJ>h>(z-2)J$ in any lattice. (This is consistent with the numerical predictions, and it includes the linear chain result $\Gamma_G=4J-2h, A_G=3/2$) [27].

Case (b). This includes $(d>1)$-dimensional lattices in the next regime $(z-2)J>h$.

Now, as well as $R^+(-z)$, the second flip-up rate, $R^+(-(z-2))$ becomes very small. The geometry of the domains of n and $n\pm 1$ sites determines the numbers m in the rates $R^+(m)$ occurring in the equation for $|n\rangle$. In particular the size q of the smallest ring of bonds on the lattice determines as $q-2$ the number of successive equations in which the only up rate is $R^+(-(z-2))$. The consequence for the gap is that s is proportional to $R^+(-z)[R^+(-(z-2))]^{q-2}$, giving the result

$$\Gamma_G = 2(zJ-h)+2(q-2)[(z-2)J-h], \tag{30}$$

where $q=4$, 6, and 3 for square, honeycomb, and triangular lattices. These results agree with the numerical ones.

The determination of the A's is most easily carried out by considering the (first order, nonlinear) recurrence relations for $\mu_n=|n\rangle/|n-1\rangle$. In the low temperature limit, ratios of small rates make the deciding μ_n's tend to 1, for the $(q-2)$ lowest n's, and to 0 for the next one; and in the limit the ratios of the coefficients c_n, d_n in that range of n's determine the numerical factor in $(1-\mu_1)$ and hence A_G. The (analytic, numerical) results are $A_G=[3/8, 0.4(3)]$, $[1/6, 0.1(6)]$, and $[1/3, 0.4(5)]$ for square, honeycomb, and triangular lattices, respectively; the agreement is good except for the last one.

The boundaries of the region are set by where new combinations of rates $R^{\pm}$ become limiting. The analytically determined ranges of validity of the results in this case (b) are $4J>h>2J$ for triangular, $2J>h>J$ for square, and $J>h>J/2$ for the honeycomb lattice.

Case (c). For the triangular lattice there is a further regime $(2J>h)$ where yet another up-flip rate, namely, $R^+(-(z-4))$, becomes small.

Here we expect, in analogy to the argument and results given above for the previous regime, that s will be proportional to $R^+(-z)[R^+(-(z-2))]^{q-2}[R^+(-(z-4))]^Q$ with Q an integer related to topological features of the triangular lattice. This gives the form

$$\Gamma_G = 2(zJ-h)+2(q-2)[(z-2)J-h]+2Q[(z-4)J-h] \tag{31}$$

(with $z=6$, $q=3$). The numerical results are consistent with this with $Q=3$.

B. Modified Glauber dynamics

Procedures for the MG dynamics are in principle similar. But now the primitive rate $R^+(-z)\sim e^{-2\beta zJ}$ is always small, in all regimes (even h very large), so always

$$\Gamma_{MG} \neq 0. \tag{32}$$

For the following we use the notation $\epsilon=R^+(-z)$; $\Delta=R^+(-(z-2))$; $\gamma=R^+(-(z-4))$; $\delta=R^-(-z)\sim R^-(-(z-2))$; $\mu_n=|n\rangle/|n-1\rangle=(1-\lambda_n)$. Then for any lattice the first two recurrence equations are

$$s=\epsilon\lambda_1, \tag{33}$$

$$z\Delta\lambda_2=\delta\lambda_1/\mu_1+s. \tag{34}$$

After these, the equations become lattice dependent; e.g., for the triangular lattice the next ones are

$$2\gamma\lambda_3=2\delta\lambda_2/\mu_2+s, \tag{35}$$

$$3\gamma\lambda_4 = 3\delta\lambda_3/\mu_3 + s, \tag{36}$$

$$4\gamma\lambda_5 = 3\delta\lambda_4/\mu_4 + s, \tag{37}$$

etc. Details of the further reductions depend on the field regime.

Case (a). For $h>(z-2)J$, the rates satisfy $\delta \ll \Delta \ll \gamma$.

Then for all the lattices the equations give two possible forms of solution: $\lambda_n \ll 1$, so $\mu_n \sim 1$ and $s=0$ (ground state); or $\mu_n \ll 1$, so $s=\epsilon \sim e^{-2\beta zJ}$. Hence

$$\Gamma_{MG} = 2zJ, \quad A_{MG} = 1. \tag{38}$$

This applies for any lattice, including the linear chain.

Case (b). In the next regime $(z-4)J<h<(z-2)J$, possible in $(d>1)$-dimensional lattices, the rate ordering is $\Delta \ll \delta \ll \gamma$.

First consider the specific case of the triangular lattice. Again because $\delta \ll \gamma$, for $s \neq 0$ the higher equations of the hierarchy give $\lambda_n \sim 1$, $n=2,3,\ldots$. But now $\Delta \ll \delta$, so the second equation of the hierarchy gives $\lambda_1 = z\Delta/\delta$ and it follows that $s=z\epsilon\Delta/\delta$. Hence

$$A_{MG} = 1/z, \quad \Gamma_{MG} = 2Jz + 2J(z-2) - 2h = 20J - 2h, \tag{39}$$

for the triangular lattice in this regime.

For the other lattices, a cycle of $(q-2)$ successive equations (after the first equation) involve Δ/δ and that is the origin of the general form

$$\Gamma_{MG} = 2zJ + 2(q-2)[(z-2)J - h]. \tag{40}$$

The (analytic, numerical) results for A_{MG} for $(z-2)J>h$ are $[1/8, 0.2(3)]$, $[1/6, 0.1(3)]$, and $[1/6, 0.3(4)]$ for square, honeycomb, and triangular lattices, respectively.

Case (c). This is on the boundary $h=(z-2)J$ between the last two regimes. Here the (analytic, numerical) results for A_{MG} are $[11/8, 1.4(2)]$, $[11/6, 1.6(6)]$, and $[7/6, 1.1(6)]$ for square, honeycomb, and triangular lattices, respectively.

Concerning the issue as to whether Γ and A can be calculated for arbitrarily smaller h's, notice that more and more cluster amplitudes occur in the coupled eigenvalue equations. This makes their exact calculation difficult beyond the regimes already treated. In particular, the A's are more difficult to calculate exactly than the Γ's because, in the coupled eigenvalue equations, coefficients related to details of cluster symmetries and surface geometry, etc., are needed for the calculation of the A's (but not for the Γ's). Also, the cluster amplitudes occurring in the coupled eigenvalue equations are those that are of the same (dominant) order in the low temperature ordering scheme. On the low field boundary of a regime additional clusters typically become of comparable order, and all their amplitudes are needed in the determination of the A's.

V. CONCLUSIONS

The low temperature relaxational kinetics of Ising ferromagnets in a field has been treated for various lattices for both Glauber and modified Glauber processes using a quantum representation of the evolution operators. The unsymmetrized version is convenient for the analytical work in the low temperature limit (Sec. IV) while the recursive numerical approach (Sec. III) requires the symmetrized form produced by a special spin rotation.

The gross features produced by the two approaches agree completely. Those features include striking differences between the Glauber and modified Glauber cases. The latter case is always activated, even at high fields. In each of a sequence of field regimes, for both processes Γ is found to be a linear function of h and the amplitude A is a constant, but both A and the form of Γ, and also the field regimes, differ between Glauber and modified Glauber cases.

While A and the slope of $\Gamma(h)$ are discontinuous at regime boundaries, Γ is continuous. This can be understood from the analytic discussion, where it is seen that the regimes are distinguished by which rates are most limiting, and in the low temperature limit the exponents in the limiting rates cross over at the regime boundaries, and those exponents determine Γ but not A.

Both the numerical and analytic investigations make no use of the shape of critical droplets nor of the most probable path toward a nucleation event, and were carried out for square, triangular, and honeycomb lattices. The numerical approach indicates, and the analytic one confirms, that Γ is lattice dependent (except in the nonactivated high field regime of the Glauber case, where it is zero), and also A is lattice dependent except in the highest field regime for the modified Glauber case. According to the analytic work, for the highest field activated regime the lattice dependence of Γ involves just the coordination number z for both Glauber and modified Glauber cases, but in subsequent regimes other geometrical aspects of the lattice, e.g., the smallest ring size q, affect the value of Γ. Similarly the lattice dependence of A is, as one moves down the field regimes, first through z, and thereafter involving further aspects of the lattice.

The quantitative agreement between the predictions of the numerical and analytic approaches is very good for Γ, and for the regime ranges, and slightly less good for A, particularly for the smallest field regimes. This is as might be expected, since (i) at low temperatures a given (but bounded) numerical error in the gap evaluation will mostly propagate an error in A, rather than in Γ, as the latter carries an extra weight proportional to β; and (ii) as h decreases the gap becomes smaller, and so does the accuracy of the machine calculations. This drawback also precludes to examine much lower temperatures than those considered throughout. To understand more fully the comparisons between the numerical and analytic results it would be desirable to generalise the analytic work to finite low temperatures.

The analytic work includes predictions for arbitrary lattices (e.g., for the regimes in which the results for Γ, A depend only on z). It would be valuable to extend this, and to extend the numerical work to other, especially three-dimensional, lattices. Further suggested extensions of the work are to other models (e.g., Potts models, where domain walls remain sharp) and to disordered cases: even a low concentration of weak bonds can make nucleation much faster. Also, it would be interesting to apply our methodology to more realistic dynamics including microscopic barriers, such as those recently studied in Ref. [10].

ACKNOWLEDGMENTS

We thank M. A. Novotny and P. A. Rikvold for helpful observations and correspondence. This work was supported by EPSRC under the Oxford Condensed Matter Theory Grants No. GR/R83712/01 and No. GR/M04426. M.D.G. acknowledges financial help and kind hospitality of the Department of Theoretical Physics, Oxford, U.K., where the later stages of this work were carried out. Support of CONICET, Argentina (Grants No. PEI 1163 and No. PIP 2763), is acknowledged.

[1] For comprehensive reviews and a literature list consult, P. A. Rikvold and B. M. Gorman in *Annual Reviews of Computational Physics*, edited by D. Stauffer (World Scientific, Singapore, 1994), Vol. 2; D. W. Oxtoby, J. Phys.: Condens. Matter **4**, 7627 (1992); J. D. Gunton and M. Droz, *Introduction to the Theory of Metastable and Unstable States* (Springer, Berlin, 1983); J. D. Gunton, M. San Miguel, and P. S. Sahni, in *Phase Transitions and Critical Phenomena*, edited by C. Domb and J. L. Lebowitz (Academic, New York, 1983), Vol. 8.

[2] S. Auer and D. Frenkel, Nature (London) **409**, 1020 (2001); N. Combe, P. Jensen, and A. Pimpinelli, Phys. Rev. Lett. **85**, 110 (2000).

[3] A. B. C. Patzer, A. Gauger, and E. Sedlmayer, Astron. Astrophys. **337**, 847 (1998).

[4] A. J. Leggett, Phys. Rev. Lett. **53**, 1096 (1984).

[5] E. Jordão Neves and R. H. Schonmann, Commun. Math. Phys. **137**, 209 (1991).

[6] E. Scoppola, Physica A **194**, 271 (1993); J. Stat. Phys. **73**, 83 (1993).

[7] R. Kotecký and E. Olivieri, J. Stat. Phys. **75**, 409 (1994).

[8] E. Olivieri and E. Scoppola, J. Stat. Phys. **79**, 613 (1995).

[9] F. Martinelli, E. Olivieri, and E. Scoppola, J. Stat. Phys. **61**, 1105 (1990).

[10] G. M. Buendía, P. A. Rikvold, K. Park, and M. A. Novotny, J. Chem. Phys. **121**, 4193 (2004).

[11] K. Park, P. A. Rikvold, G. M. Buendía, and M. A. Novotny, Phys. Rev. Lett. **92**, 015701 (2004).

[12] K. Brendel, G. T. Barkema, and H. van Beijeren, Phys. Rev. E **71**, 031601 (2005).

[13] V. A. Shneidman and G. M. Nita, Phys. Rev. E **68**, 021605 (2003); Phys. Rev. Lett. **89**, 025701 (2002).

[14] M. A. Novotny, Comput. Phys. Commun. **147**, 659 (2002); see also the related algorithm of A. B. Bortz, M. H. Kalos, and J. L. Lebowitz, J. Comput. Phys. **17**, 10 (1975).

[15] K. Park, M. A. Novotny, and P. A. Rikvold, Phys. Rev. E **66**, 056101 (2002).

[16] A. Bovier and F. Manzo, J. Stat. Phys. **107**, 757 (2002).

[17] N. G. van Kampen, *Stochastic Processes in Physics and Chemistry*, 2nd ed. (North-Holland, Amsterdam, 1992).

[18] R. J. Glauber, J. Math. Phys. **4**, 294 (1963); P. A. Martin, J. Stat. Phys. **16**, 149 (1977).

[19] A description related to this situation is studied by H. van Beijeren, J. Stat. Phys. **110**, 1397 (2003), where nucleation is thought of as a diffusion process in a potential well with escape over a barrier.

[20] J.-S. Wang, Physica A **161**, 249 (1989); F. Martinelli, E. Olivieri, and E. Scoppola, J. Stat. Phys. **62**, 135 (1991).

[21] This dynamic was also studied by P. A. Rikvold and M. Kolesik, J. Phys. A **35**, L117 (2002), in the context of field-driven interfaces.

[22] J. Lothe and G. M. Pound, J. Chem. Phys. **36**, 2080 (1962); H. Reiss, J. Katz, and E. Cohen, *ibid.* **48**, 5553 (1968); V. Ruth, J. P. Hirth, and G. M. Pound, *ibid.* **88**, 7079 (1988).

[23] Consult G. H. Golub and C. F. van Loan, *Matrix Computations*, 3rd ed. (Johns Hopkins University Press, Baltimore, 1996).

[24] At a coarse grained or hydrodynamic level of description this corresponds to the so-called model A in the classification scheme of P. C. Hohenberg and B. Halperin, Rev. Mod. Phys. **49**, 435 (1977).

[25] Certainly, for $h=0$ both dynamics coincide except for a factor 2, which is retained to follow the notation of Ref. [11].

[26] I. S. Gradshteyn and I. M. Ryzhik, *Table of Integrals, Series and Products*, 5th ed. (Academic Press, San Diego, 1994).

[27] For exact results in Ising chains evolving with a related dynamic under magnetic fields consult H. J. Hilhorst, Physica A **97**, 171 (1975).